

Optical Characterization of Double Perovskite $\text{Ba}_2\text{FeNbO}_6$ Powders Derived from Molten Salt Method

Yao Lu, Xiangxiao Meng, Zhipeng Pei, Kai Leng, Weiren Xia, Xinhua Zhu*

National Laboratory of Solid State Microstructures, School of Physics, Nanjing University, Hankou Road 22, Nanjing 210093, China

*Corresponding author: E-mail: xhzhu@nju.edu.cn; Tel.: (+86) 025-83592772

DOI: 10.5185/amlett.2020.091554

Double perovskite $\text{Ba}_2\text{FeNbO}_6$ (BFN) powders were synthesized by molten salt method. Their optical properties were characterized by UV-Vis absorption spectra, and the band gaps (E_g) were determined to be 2.12 - 2.25 eV. The E_g values were tuned by adjusting the processing parameters of molten-salt route (e.g., annealing temperature, holding time as well as the molten salt ratios). The varied E_g values are ascribed to the different content ratios of Fe^{3+} to Fe^{2+} ions and the oxygen vacancies in the BFN powders. Oxygen vacancies in the BFN powders result in the distortions of FeO_6 octahedrons, leading to different Fe-O bond lengths. Thus, the overlapping between the O-2p and Fe-3d orbitals is changed, making the E_g values changed. A small absorption shoulder with absorption edge at 650 nm ($E_g \sim 1.91$ eV) observed in the BFN powders, was ascribed to the d-d electronic transition from the Fe 3d- b_{2g} to Fe 3d- b_{1g} orbitals, which were formed by further splitting of Fe 3d orbitals in the distorted octahedral field. The present work offers an effective approach to tuning the E_g of BFN powders, which find promising applications in the fields of photovoltaic and photocatalytic devices.

Introduction

In recent years, the development and utilization of solar energy in environmental remediation and water splitting have been widely studied worldwide, which have become one of the most important topics in the fields of photocatalytic researches [1,2]. Massive efforts have been made to develop non-toxic, low-cost, efficient and stable photocatalysts for water splitting and environmental remediation. Up to date, many kinds of photocatalysts based on metal oxides, sulphides and (oxy) nitrides with different structures and compositions have been reported [3-8]. Among them, perovskite oxides (ABO_3) and their derivatives (layered perovskite oxides) are ideal photocatalysts for water splitting because they exhibit excellent photocatalytic properties in the UV region [4-8]. However, they exhibit low solar-to-hydrogen conversion efficiencies under visible light irradiation, although they are stable in aqueous solutions and resistant to oxidation. Such underperformance is mainly ascribed to their too wide band gaps (3 - 5 eV) to effectively absorb the main portion of the sunlight spectrum, i.e., visible light. Therefore, in order to develop more efficient visible-light photocatalysts, much attention has been paid to double perovskite oxides with a general formula of $\text{A}_2\text{B}'\text{B}''\text{O}_6$ (A: rare earth ions, B', B'': transition metals), where the narrow band gaps can be realized by using two different transition-metal cations occupied at the B' and B'' sites in double perovskite oxides, leading to the B-sited cation off-center displacements due to the different ionic radii [6]. In addition, the band gaps of double perovskite oxides can be also effectively reduced by

using their chemical flexibilities rather than incorporating anion impurities or transition metal impurities (with d^{10} orbitals or partially filled d^n orbitals) [9]. For example, in the double perovskite $\text{Ba}_2\text{BiNbO}_6$, the Bi-rich and Nb-poor off stoichiometry (i.e., $\text{Ba}_2\text{Bi}_{1+x}\text{Nb}_{1-x}\text{O}_6$) can significantly reduce the band gap to 1.64 eV in a form of film with a composition of $\text{Ba}_2\text{Bi}_{1.4}\text{Nb}_{0.6}\text{O}_6$ [9]. As for multiferroic double perovskite $\text{Bi}_2\text{FeCrO}_6$, its band gap can be tuned effectively by engineering the cationic ordering at B-sites [10,11]. Such strategy can be further used in developing visible-light photocatalysts based on double perovskite oxides. Besides the promising applications as visible-light photocatalysts, double perovskite oxides also exhibit a wide range of multifunctional properties (e.g., magnetic insulating [12-14], half-metallic ferromagnetic [15-17], ferromagnetic [18], antiferromagnetic [19], ferroelectric [20,21], magneto-dielectric [22,23], and multiferroic properties [24,25]), which enable double perovskite oxides to be applicable in a broad spectrum of fields such as oxide spin electronics, energy, environment, and health [26-28].

Double perovskite oxides with various combination of A, B', and B'' cations have been studied by different authors [29-33]. Many of them are highly ordered double perovskites, with predominant antiferromagnetic interactions and/or magnetic frustration due to the different competing magnetic interactions in these materials. That can be ascribed to the different kinds of structural distortions and order/disorder between B' and B'' cations. Furthermore, band structure calculations indicate that some of them are half-metallic ferromagnets with relatively high

Curie temperature [34], and they exhibit large low-field room temperature magnetoresistance [15]. The local spin density calculations also predict that half-metallic characteristics exist in some of the antiferromagnetic (AFM) double perovskites [35]. As lead-free double perovskite and eco-friendly materials, $\text{Ba}_2\text{FeNbO}_6$ (BFN) compounds attract much attention of researchers due to their high dielectric constant ($\sim 10^4$) over a wide temperature range (100 - 600 K), which have important applications in the fields of capacitors, sensors, and memory devices [36,37]. The origins of the high dielectric constant in the BFN system are ascribed to grain boundary effect, space charge effect, electron hopping, Maxwell-Wagner type interfacial and dipolar polarizations [38-42]. The relaxor-like dielectric behavior observed in the BFN double perovskite ceramics is attributed to the thermally induced oxygen vacancies and enhanced electrons hopping between the localized carriers [43,44]. The magnetic properties of BFN double perovskite ceramics is also reported, which is an antiferromagnetic insulator with $T_N = 25$ K and exhibits a weak ferromagnetic behavior at 5 K [45,46]. Narrow optical band gaps (~ 1.30 eV) are also reported in the La-modified BFN double perovskite ceramics, and a broad diffusion absorption bands was observed in the wavelength of 200 - 900 nm [38]. Such narrow band gaps of these La-modified BFN double perovskite ceramics make them promising candidate used for the photocatalyst and solar cells. In addition, the structural, electrical and optical properties of BFN thin films are also investigated [47-49]. The band gap of the BFN thin films was reported to be 1.37 eV, indicating that the BFN films can be used as photocatalyst and other photoelectric devices.

Despite plenty of works have been reported on the BFN ceramics and thin films, there are still few works reported on the BFN powders [50-52]. In our previous study, we reported on the synthesis of BFN powders at low temperatures by molten-salt synthesis (MSS) method [52]. The effects of MSS processing parameters (e.g., annealing temperature, holding time as well as the molten salt ratios) on the microstructure, dielectric and magnetic properties of the BFN double perovskite powders were systematically investigated. To explore the potential applications of BFN powders in the technical fields of photovoltaic and photocatalytic devices, the optical properties of BFN powders are investigated by UV-Vis spectroscopy in this work. The optical band gaps (E_g) of the BFN powders were deduced from their UV-Vis absorption spectra. It is found that the E_g values of BFN powders can be tuned in the range of 2.12 - 2.25 eV by adjusting the MSS processing parameters (e.g., annealing temperature, holding time as well as the molten salt ratios). A possible electronic band structure of BFN is proposed to interpret their optical properties.

Experimental

In this work, BFN double perovskite powders were synthesized by MSS method from the reagent grad BaCO_3 , Fe_2O_3 , Nb_2O_5 , SrCO_3 and TiO_2 powders (Sigma-Aldrich,

Shanghai, China). The eutectic mixed NaCl-KCl salts with analytical grade reagent were used as molten salt medium. Details for the synthesis of BFN powders by MSS method were described elsewhere [52]. Three group samples (A-C) were synthesized at different conditions, details are given out in Table 1. For the synthesis of the BFN- SrTiO_3 solid solution powders by MSS method, analytical pure BaCO_3 , Fe_2O_3 , Nb_2O_5 , SrCO_3 and TiO_2 were used as raw materials and the eutectic mixed NaCl-KCl salt were used as molten salt medium.

Phase structures of the BFN powders were examined by X-ray powder diffraction (XRD) using Cu-K α radiation at $\lambda = 1.54056$ Å. The morphology and grain size of the BFN double perovskite powders were characterized by a scanning electron microscope (SEM) (S-3400N II, Hitachi) equipped with an X-ray energy dispersive spectroscopy (EDS) (EX-250 spectroscopy, HORIBA Corporation) for chemical composition analyses. The UV-Vis absorption spectra of the BFN powders were measured in the reflection geometry by the UV-Vis spectrophotometer (Shimadzu, UV2550) at room temperature. The measured diffuse reflectance spectra are used to estimate the absorbance according to the standard Kubelka-Munk theory, which is based on the assumption of multiple scattering, describing the optical behaviour of materials with small particles that scatter and absorb radiant energy. The Kubelka-Munk equation expresses the reflectance or transmittance in terms of an absorption coefficient, $\alpha(E)$, and a scattering coefficient, S . It is known that the absorption coefficient $\alpha(E)$ in a solid is contributed from both the direct and the indirect band gap transitions [53], which is given as

$$\alpha(E) = \frac{A}{E}(E - E_{g,\text{dir}})^{0.5} + \frac{B}{E}(E - E_{g,\text{indir}} \mp E_{\text{ph}})^2 \quad (1)$$

where $E_{g,\text{dir}}$ and $E_{g,\text{indir}}$ are the magnitudes of direct and indirect band gaps, respectively, E_{ph} is the emitted (or absorbed) phonon energy, and A and B are constants. While assuming a simple band shape this model allows for extracting the direct optical energy gap ($E_{g,\text{dir}}$) by plotting $(\alpha E)^2$ versus the photon energy E . In contrast, plotting $(\alpha E)^{0.5}$ as a function of the photon energy E and linear extracting $(\alpha E)^2 = 0$ gives the indirect optical energy gap ($E_{g,\text{indir}}$) [54]. In this work, we focus on the direct optical band gaps (E_g) of the BFN powders, which are obtained by using the Tauc equation [54]:

$$(\alpha E)^2 = A (E - E_g) \quad (2)$$

where E is the incident photon energy, A is the absorption edge width parameter.

Results and discussion

Ultraviolet-visible (UV-Vis) spectroscopy is used for determining band structures of semiconductors. It further amounts response of the sample to UV and visible range of electromagnetic radiations. Fig. 1 shows the UV-Vis optical absorption spectra of the group A samples synthesized at different temperatures, and the corresponding plots of $(\alpha E)^2$ vs E . It is observed in

Fig. 1(a) that the wavelength corresponding to the optical absorption peak has a red shift (from 390 nm to 447 nm) as increasing the annealed temperature from 800°C to 1100°C. Details are shown in the inset of **Fig. 1(a)**. That is attributed to the larger particle sizes of the BFN powders synthesized at higher temperatures [52]. A small absorption shoulder with absorption edge around 650 nm ($E_g \sim 1.91$ eV) was also observed in the BFN powders (A800) synthesized at 800°C. In order to determine the direct band gap energy of the BFN powders, in **Fig. 1(b)** we perform the linear extrapolations of $(\alpha E)^2$ vs E plots to $(\alpha E)^2 = 0$, yielding the direct band gaps, which are in the range of 2.18 - 2.23 (± 0.06) eV. These E_g values are close to that ($E_g = 2.29$ eV) reported by Zhang *et al.* [50]. The obtained optical band gap energy corresponds to the energy difference between the valence band maximum (VBM) and the conduction band minimum (CBM). Detailed discussions will be given in the following section.

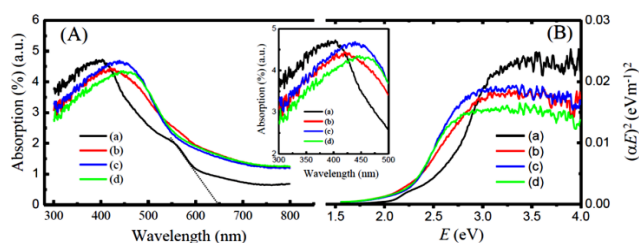


Fig. 1. (A) Optical absorption spectra of the group A samples synthesized at different temperatures. (a) 800°C, (b) 900°C, (c) 1000°C, and (d) 1100°C. Inset is the local optical absorption spectra, indicating the red shift of the wavelength corresponding to the optical absorption peak. (B) Corresponding plots of $(\alpha E)^2$ vs E curves.

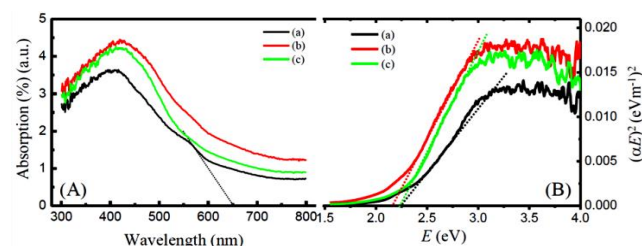


Fig. 2. (A) Optical absorption spectra of the group B samples synthesized at 900°C with different holding time. (a) 2 h, (b) 5 h, and (c) 8 h. (B) Corresponding plots of $(\alpha E)^2$ vs E curves.

Similarly, the optical absorption spectra of the group B samples (synthesized at 900°C with different holding time)

are also measured, as shown in **Fig. 2(a)**, and their optical band gaps are determined from the corresponding plots of $(\alpha E)^2$ vs E curves shown in **Fig. 2(b)**. As shown in **Fig. 2(a)**, the optical absorption peak had a red shift (from 395 nm to 420 nm) as increasing the holding from 2 h to 5 h but remained the same position as the holding time was increased up to 8h. Similarly, small absorption shoulder with absorption edge around 650 nm ($E_g \sim 1.91$ eV) was observed in the BFN powders synthesized at 800°C with holding time of 2 h. The E_g values of the BFN powders synthesized at 900°C with holding time of 2, 5, and 8 h, were deduced from the $(\alpha E)^2$ vs. E graphs, which was 2.25, 2.18, and 2.25 eV, respectively. The direct optical band gaps of the BFN powders can be also tuned by using different molten salt ratios, which is also investigated in this work. The optical absorption spectra of the group C samples are shown in **Fig. 3(a)**, and the corresponding plots of $(\alpha E)^2$ vs. E curves are shown in **Fig. 3(b)**. With increasing the molar ratios of $\text{BaCO}_3:\text{Fe}_2\text{O}_3:\text{Nb}_2\text{O}_5:\text{NaCl}:\text{KCl}$ from 4:1:1:20:20 to 4:1:1:100:100, the wavelength corresponding to the optical absorption peak had a blue shift (from 463 nm to 453 nm) due to the reduction of the average particle size from 480 to 310nm (seen in **Table 1**)[52], and the E_g values of the group C samples were increased from 2.12 eV to 2.23 eV. The direct optical band gaps of the BFN powders synthesized at different conditions are summarized in **Table 1**. It is found that the E_g values of the BFN powders can be tuned in the range of 2.12eV-2.25eV by adjusting the MSS processing parameters (e.g., annealing temperature, holding time as well as molten salt content), which enables the BFN powders to be used as visible-light photocatalysts in the application fields of photovoltaic and photocatalytic devices.

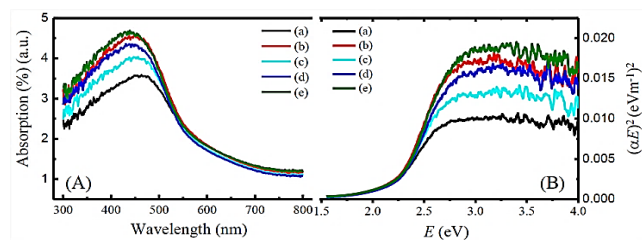


Fig. 3. (A) Optical absorption spectra of the group C samples synthesized at 1000°C for 5 h under the molar ratios of $\text{BaCO}_3:\text{Fe}_2\text{O}_3:\text{Nb}_2\text{O}_5:\text{NaCl}:\text{KCl}$ equal to (a) 4:1:1:20:20, (b) 4:1:1:40:40, (c) 4:1:1:60:60, (d) 4:1:1:80:80, and (e) 4:1:1:100:100. (B) Corresponding plots of $(\alpha E)^2$ vs E curves.

Table 1. Three group (A-C) $\text{Ba}_2\text{FeNbO}_6$ powders synthesized by MSS method, their EDS data, average particle size and direct optical band gaps (E_g).

Sample group	Annealing Temperature (°C)	Holding time (h)	Ratio of molten salt ($\text{BaCO}_3:\text{Fe}_2\text{O}_3:\text{Nb}_2\text{O}_5:\text{NaCl}:\text{KCl}$)	Atomic percentage (%) ($\text{Ba}:\text{Fe}:\text{Nb}$) ^{a)}	Cation molar ratio ($\text{Ba}:\text{Fe}:\text{Nb}$)	Average grain size (nm)	Optical band gap E_g (eV) ^{b)}
A800	800			20.23:10.43:9.75	2:1.03:0.96	165	2.22
A900	900			21.58:11.01:10.47	2:1.02:0.97	300	2.18
A1000	1000	5	4:1:1:100:100	19.26:9.92:9.63	2:1.03:1.00	500	2.23
A1000	1100			20.92:10.88:10.25	2:1.04:0.98	525	2.19
B2		2	4:1:1:100:100	21.65:11.15:10.61	2:1.03:0.98	200	2.25
B5	900	5		21.58:11.01:10.47	2:1.02:0.97	300	2.18
B8		8		22.26:10.74:10.72	2:1.01:0.99	355	2.25
C20			4:1:1:20:20	24.08:10.58:10.68	2:0.88:0.88	480	2.12
C40			4:1:1:40:40	20.91:10.77:10.21	2:1.03:0.97	475	2.22
C60	1000	5	4:1:1:60:60	22.56:11.37:10.52	2:1.01:0.93	410	2.19
C80			4:1:1:80:80	22.83:10.98:10.40	2:0.96:0.91	395	2.22
C100			4:1:1:100:100	20.60:10.51:10.31	2:1.02:1.00	310	2.23

^{a)}The error bar for EDS data of compositions: Ba: $\pm 2\%$; Fe: $\pm 5\%$; Nb: $\pm 5\%$; ^{b)}the error bar for the direct optical band gap E_g is ± 0.06 eV.

The optical band gaps of BFN powders are determined from the energy difference between the VBM and the CBM, which are closely related to the electronic structures. The electronic structures of the perovskite transition metal oxides are generally defined by the d -level of the transition metal and the $2p$ -level of the O atoms, when composed of d^0 transition metals like Ti^{4+} , Nb^{5+} and Ta^{5+} . However, in the perovskite oxides containing transition metals with the d orbitals partly occupied, their electronic structures should be strongly influenced by those transition ions with partly occupied d orbitals [6]. Basically, in the ferroelectric perovskite oxide, the VBM arises mainly from the O- $2p$ orbitals, while the CBM is essentially set by B-site transition metal d orbitals. Compared to the A-cation, the B-cation has a much more significant effect on fixing the band gaps of perovskite ABO_3 oxides [55,56]. In the present BFN powders, the Nb and Fe metal ions occupy the octahedral sites at random with some oxygen vacancies in ordered or disordered distribution. The Fe^{3+} ions with electronic configuration of $3d^54s^0$ (high spin configuration) reside at the center of the Fe-O octahedrons with partly oxygen vacancies, their five degenerate $3d$ orbitals would be split by the octahedral crystal field into two parts, an lower energy level of 6-fold degenerate t_{2g} orbitals (d_{xy} , d_{yz} , and d_{zx}) and a 4-fold higher energy level of e_g orbitals ($d_{x^2-y^2}$ and d_{z^2}). The distorted Fe-O octahedrons (an elongated oxygen octahedron or compressed oxygen octahedron) with the random oxygen vacancies make it possible for the further splitting of the e_g and t_{2g} orbitals. The e_g orbitals will be split into a higher energy b_{1g} ($d_{x^2-y^2}$) orbital and a lower-energy a_{1g} (d_{z^2}) orbital, and the t_{2g} orbitals with 6-fold degenerate will be further split into a higher energy b_{2g} (d_{xy}) orbital and a lower 4-fold degenerate e_g (d_{yz} , d_{zx}) orbitals, which are schematically shown in Fig. 4(a). The excitation energy from t_{2g} to e_g orbital is called Δ_o (or $10 Dq$), its theoretical value is calculated to be 1.80 eV in $LaFeO_3$ and $SrFeO_3$ [57]. The split Fe $3d-t_{2g}$ and Fe $3d-e_g$ orbitals and their further splitting due to the distorted octahedron should play important roles in constructing the band structures of BFN powders. Therefore, in the BFN powders, the VBM consists of the hybridized Fe $3d-e_g$ and O- $2p$ orbitals, and while the CBM is formed by the hybridization of Nb- $4d$ and Fe $3d-b_{1g}$ orbitals. Despite Ba atoms offer electrons to keep the system charge balanced, however, they do not make a contribution to the VBM or CBM, like the case of the Ba_2BiNbO_6 compound [9]. A schematic diagram of the band structure of the BFN is shown In Fig. 4(b). The direct optical band gaps of the BFN powders (in the range of 2.12 - 2.25 eV) correspond to the electronic transition from the valence band to conduction band. The variations of the E_g values for the BFN powders can be attributed to the different content ratios of Fe^{3+} to Fe^{2+} and the oxygen vacancies, as revealed by the XPS spectra [52]. The oxygen vacancies in the BFN powders would lead to the distortions of FeO_6 octahedrons (e.g., an elongated oxygen octahedron), thus, the Fe-O bond lengths became shorter in the ab plane

whereas longer in the c direction. Therefore, the overlapping between the O- $2p$ and Fe- $3d$ orbitals is changed, resulting in the varied E_g values of the present samples in the range of 2.12 - 2.25 eV. The small absorption shoulder with absorption edge at 650 nm ($E_g \sim 1.91$ eV) can be ascribed to the $d-d$ electronic transition from the Fe $3d-b_{2g}$ to Fe $3d-b_{1g}$ orbitals, which are formed by the further splitting of Fe $3d$ orbitals due to the distorted octahedral crystal field. Similar case was reported in the antiferromagnetic $CaFe_2O_4$ compound, where its band gap energy was calculated to be about 1.9 eV, and it was increased by including the on-site Coulomb interaction between the d -electrons that enhances the splitting between the filled and empty orbitals in Fe $3d$ manifold [58]. More experiments are needed to reveal the exact band structure of the BFN photocatalysts.

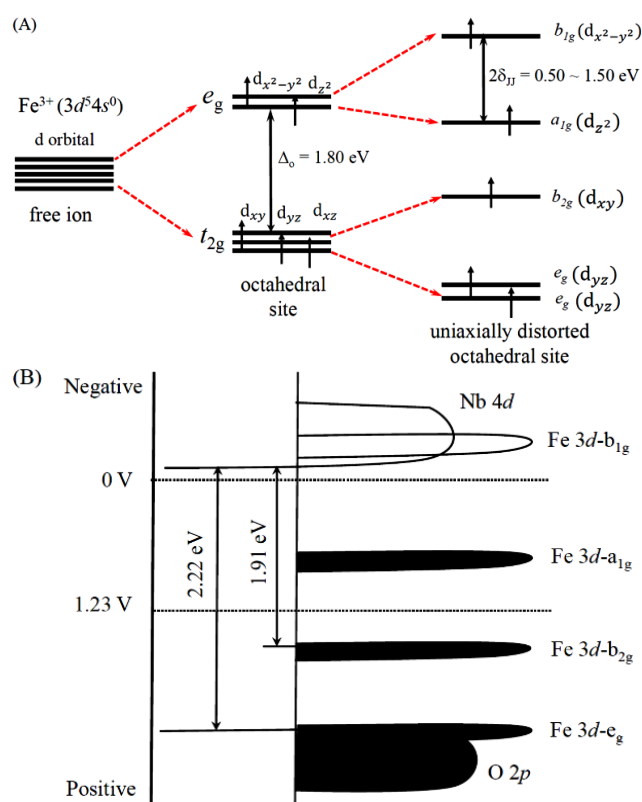


Fig. 4. Schematic diagrams showing (A) 3d orbitals of Fe^{3+} ions ($3d^54s^0$, high spin configuration) splitting under different ligand fields and (B) the band structure of the Ba_2FeNbO_6 , respectively.

Conclusion

Double perovskite BFN powders were synthesized by molten-salt method. Their optical properties were characterized by UV-Vis spectroscopy. The optical E_g values of the BFN powders deduced from their UV-Vis spectra, were in the range of 2.12 eV - 2.25 eV, which can be adjusted by controlling the processing parameters of molten-salt route. The direct optical band gaps of the BFN powders are associated with the electronic transition from the valence band (formed by the hybridized Fe $3d-e_g$ and O- $2p$ orbitals) to conduction band (formed by the

hybridization of Nb-4d and Fe 3d-b_{1g} orbitals). The varied E_g values of the BFN powders can be ascribed to the different content ratios of Fe³⁺ to Fe²⁺ and the oxygen vacancies. The oxygen vacancies in the BFN powders produce the distortions of FeO₆ octahedrons, leading to different Fe-O bond lengths, thus, the overlapping between the O-2p and Fe-3d orbitals changed, resulting in the varied E_g values of the present samples. The observed small absorption shoulder with absorption edge around 650 nm (E_g ~ 1.91 eV) is ascribed to the d-d electronic transition from the Fe 3d-b_{2g} to Fe 3d-b_{1g} orbitals, which are formed via the further splitting of Fe 3d orbitals because of the distorted octahedral crystal field. The present works provide an effective approach to tuning the optical band gaps of double perovskite BFN powders, which have promising applications in the fields of photovoltaic and photocatalytic devices.

Acknowledgements

The authors acknowledge the financial supports from National Natural Science Foundation of China (grant Nos. 11674161 and 11974170), Natural Science Foundation of Jiangsu Province (grant No. BK20181250), and undergraduate teaching reform project from Nanjing University (grant No. X20191028402).

Conflicts of interest

The authors declare that they have no competing interests.

Keywords

Double perovskite, Ba₂FeNbO₆ (BFN) powders, molten salt synthesis, optical properties.

Received: 06 April 2020

Revised: 11 June 2020

Accepted: 17 July 2020

References

- Nuraje, N.; Asmatulu, R.; Kudaibergenov, S.; *Curr. Inorg. Chem.*, **2012**, *2*, 124.
- Zhang, G.; Liu, G.; Wang, L. Z.; Irvine, J. T. S.; *Chem. Soc. Rev.*, **2016**, *45*, 5951.
- Ahmed, M.; Guo, X. X.; *Inorg. Chem. Front.*, **2017**, *3*, 578.
- Jia, Q.; Iwase, A.; Kudo, A.; *Chem. Sci.*, **2014**, *5*, 1513.
- Shi, J.; Guo, L.; *Prog. Nat. Sci. Mater. Int.*, **2012**, *22*, 592.
- Grinberg, I.; West, D. V.; Torres, M.; Gou, G. Y.; Stein, D. M.; Wu, L. Y.; Chen, G. N.; Gallo, E. M.; Akbashev, A. R.; Davies, P. K.; Spanier, J. E.; Rappe, A. M.; *Nature*, **2013**, *503*, 509.
- Kanhere, P.; Chen, Z.; *Molecules*, **2014**, *19*, 19995.
- Huang, Y. B.; Liu, J.; Deng, Y. C.; Qian, Y. Y.; Jia, X. H.; Ma, M. M.; Yang, C.; Liu, K.; Wang, Z. J.; Qu, S. C.; Wang, Z. G.; *J. Semicond.*, **2020**, *41*, 011701.
- Weng, B. C.; Xiao, Z. W.; Meng, W. W.; Grice, C. R.; Poudel, T.; Deng, X. M.; Yan, Y. F.; *Adv. Energy Mater.*, **2007**, *7*, 1602260.
- Nechache, R.; Harnagea, C.; Li, S.; Cardenas, L.; Huang, W.; Chakrabarty, J.; Rosei, F.; *Nat. Photonics*, **2015**, *9*, 61.
- Quattropiani, A.; Stoeffler, D.; Fix, T.; Schmerber, G.; Lenertz, M.; Versini, G.; Rehspringer, J. L.; Slaoui, A.; Dini, A.; Colis, S.; *J. Phys. Chem. C*, **2018**, *122*, 1070.
- Iwasawa, H.; Saitoh, T.; Yamashita, Y.; Ishii, D.; Kato, H.; Hamada, N.; Tokura, Y.; *Phys. Rev. B*, **2005**, *71*, 075106.
- Feng, H. L.; Calder, S.; Ghimire, M. P.; Yuan, Y. H.; Shirako, Y.; Tsujimoto, Y.; Matsushita, Y.; Hu, Z. W.; Kuo, C. Y.; Tjeng, L. H.; Pi, T. W.; Soo, Y. L.; He, J. F.; Tanaka, M.; Katsuya, Y.; Richter, M.; Yamaura, K.; *Phys. Rev. B*, **2016**, *94*, 235158.
- Sohn, C.; Skoropata, E.; Choi, Y. S.; Gao, X.; Rastogi, A.; Huon, A.; McGuire, A. A.; Nuckols, L.; Zhang, Y. W.; Freeland, J. W.; Haskel, D.; Lee, H. N.; *Adv. Mater.*, **2019**, *31*, 1805389.
- Kobayashi, K. I.; Kimura, T.; Sawada, H.; Terakura, K.; Y. Tokura, Y.; *Nature*, **1998**, *395*, 677.
- Chen, W.; Mizumaki, M.; Seki, H.; Senn, M. S.; Saito, T.; D. Kan, D.; Attfield, J. P.; Shimakawa, Y.; *Nat. Commun.*, **2014**, *5*, 3909.
- Kato, H.; Okuda, T.; Okimoto, Y.; Tomioka, Y.; Takenoya, Y.; Ohkubo, A.; Kawasaki, M.; Tokura, Y.; *Appl. Phys. Lett.*, **2002**, *81*, 328.
- D. Serrate, D.; Teresa, J. M. D. M.; Ibarra, R.; *J. Phys.: Condens. Matter*, **2007**, *19*, 023201.
- Yan, B. H.; Paul, A. K.; Kanungo, S.; Reehuis, M.; Hoser, A.; Többsens, D. M.; Schnelle, W.; Williams, R. C.; Lancaster, T.; Xiao, F.; Möller, J. S.; Blundell, S. J.; Hayes, W.; Felser, C.; Jansen, M.; *Phys. Rev. Lett.*, **2014**, *112*, 147202.
- Parida, B. N.; Pattanayak, D. K.; Parida, R. K.; Mohanty, B.; Nayak, N. C.; *J. Mol. Struct.*, **2019**, *1189*, 288.
- Parida, B. N.; Panda, N.; Padhee, R.; Parida, R. K.; *Phase Trans.*, **2018**, *91*, 638.
- Lekshmi, P. N.; Raji, G. R.; Vasundhara, M.; Varma, M. R.; Pillai, S. S.; Valant, M.; *J. Mater. Chem. C*, **2013**, *1*, 6565.
- Mandal, P. R.; Sahoo, R.; Nath, T. K.; *Phys. B-Condens. Matter*, **2014**, *448*, 64.
- Fukushima, T.; Stroppa, A.; Picozzi, S.; Perez-Mato, J. M.; *Phys. Chem. Chem. Phys.*, **2011**, *13*, 12186.
- Nechache, R.; Harnagea, C.; Carignan, L. P.; Gautreau, O.; Pintilie, L.; Singh, M. P.; Menard, D.; Fournier, P.; Alexe, M.; Pignolet, A.; *J. Appl. Phys.*, **2009**, *105*, 061621.
- Vasala, S.; Karppinen, M.; *Prog. Solid State Chem.*, **2015**, *43*, 1.
- Pei, Z. P.; Lu, Y.; Wu, H.; Xia, W. R.; Zhu, X. H.; *J. Chin. Ceram. Soc.*, **2019**, *47*, 518.
- Hossain, A.; Ullah, A. K. M. A.; Guin, P. S.; Roy, S.; *J. Sol-Gel Sci. Technol.*, **2020**, *93*, 479.
- Chen, X. Y.; Xu, J.; Xu, Y. S.; Luo, F.; Du, Y. P.; *Inorg. Chem. Front.*, **2019**, *6*, 2226.
- Hossain, A.; Bandyopadhyay, P.; Roy, S.; *J. Alloys Compd.*, **2018**, *740*, 414.
- Knapp, M. C.; Woodwar, P. M.; *J. Solid State Chem.*, **2006**, *179*, 1076.
- Shimakawa, Y.; Azuma, M.; Ichikawa, N.; *Materials*, **2011**, *4*, 153.
- Kleibecker, J. E.; Choi, E. M.; Jones, E. D.; Yu, T. M.; Sala, B.; MacLaren, B. A.; Kepaptsoglou, D.; Hernandez-Maldonado, D.; Ramasse, Q. M.; Jones, L.; Barthel, J.; MacLaren, I.; MacManus-Driscoll, J. L.; *NPG Asia Mater.*, **2017**, *9*, e406.
- Kobayashi, K. I.; Kimura, T.; Tomioka, Y.; Sawada, H.; Terakura, K.; Tokura, Y.; *Phys. Rev. B*, **1999**, *59*, 11159.
- Pickett, W. E.; *Phys. Rev. B*, **1998**, *57*, 10613.
- Kar, S. K.; Kumar, P.; *J. Electroceram.*, **2013**, *31*, 331.
- Chung, C. Y.; Chang, Y. H.; Chen, G. J.; Chai, Y. L.; *J. Cryst. Growth*, **2005**, *284*, 100.
- Kar, S. K.; Swain, S.; Sonia; Kumar, P.; *Mater. Chem. Phys.*, **2015**, *155*, 171.
- Patel, P. K.; Yadav, K. L.; Singh, H.; Yadav, A. K.; *J. Alloys Compd.*, **2014**, *591*, 224.
- Raevski, I. P.; Prosandeev, S. A.; Bogatin, A. S.; Malitskaya, M. A.; Jastrabik, L.; *J. Appl. Phys.*, **2003**, *93*, 4130.
- Liu, Y. Y.; Chen, X. M.; Liu, X. Q.; Li, L.; *Appl. Phys. Lett.*, **2007**, *90*, 192905.
- Saha, S.; Sinha, T. P.; *J. Phys.: Condens. Mater.*, **2002**, *14*, 249.
- Wang, Z.; Chen, X. M.; Ni, L.; Liu, X. Q.; *Appl. Phys. Lett.*, **2007**, *90*, 022904.
- Sun, X. H.; Wang, C. C.; Wang, G. J.; Lei, C. M.; Li, T.; Mei, J. Y.; Cui, Y. M.; *J. Electroceram.*, **2012**, *29*, 187.
- Rama, N.; Philipp, J. B.; Opel, M.; Chandrasekaran, K.; Sankaranarayanan, V.; Gross, R.; Rao, M. S. R.; *J. Appl. Phys.*, **2004**, *95*, 7528.
- Bochenek, D.; Surowiak, Z.; Vejpravova, J. P.; *J. Alloys Compd.*, **2009**, *487*, 572.
- Yu, L.; Deng, H. M.; Zhou, W. L.; Shen, P.; Chen, S. Q.; Yang, P. X.; Chu, J. H.; *Mater. Lett.*, **2018**, *219*, 89.
- Zhang, W.; Li, L.; Chen, X. M.; *J. Appl. Phys.*, **2009**, *106*, 104108.
- Zhang, W.; Li, L.; Chen, X. M.; *J. Appl. Phys.*, **2010**, *108*, 044104.
- Zhang, G. Q.; Sun, S. R.; Jiang, W. S.; Miao, X.; Zhao, Z.; Zhang, X. Y.; Qu, D.; Zhang, D. Y.; Li, D. B.; Sun, Z. C.; *Adv. Energy Mater.*, **2017**, *7*, 1600932.

51. Köferstein, R.; Ebbinghaus, S. G.; *J. Eur. Ceram. Soc.*, **2017**, *37*, 1509.
52. Lu, Y.; Pei, Z. P.; Wu, H.; Leng, K.; Xia, W. R.; Zhu, X. H.; *J. Mater. Sci.*, **2020**, *55*, 4179
53. Pankove, J. I.; *Optical Processes in Semiconductors*, Dover, New York, **1971**.
54. Tauc J.; Grigorovici, R.; Vancu, A.; *Phys. Status Solidi*, **1966**, *15*, 627.
55. Wang, F. G.; Grinberg, J.; Rappe, A. M.; *Appl. Phys. Lett.*, **2014**, *10*, 152903.
56. Piskunov, S.; Heifets, E.; Eglitis, R.; Borstel, G.; *Comput. Mater. Sci.*, **2004**, *29*, 165.
57. Ikeno, H.; Tanaka, I.; Miyamae, T.; Mishima, T.; Adachi, H.; Ogasawara, K.; *Mater. Trans.*, **2004**, *45*, 1414.
58. Obata, K.; Obukuro, Y.; Matsushima, S.; Nakamura, H.; Arai, M.; Kobayashi, K.; *J. Ceram. Soc. Jpn.*, **2013**, *121*, 766.

Authors biography

Mr. Y. Lu received his M.S. degree in condensed matter physics in 2019 from Nanjing University under the supervision of Prof. X. Zhu. Mr. X. Meng received his B.S. degree in condensed matter physics in 2019 from Nanjing University under the supervision of Prof. X. Zhu. Mr. Z. Pei is a current M. Sci. candidate at the School of Physics, Nanjing University, under the supervision of Prof. X. Zhu. His research interests include the fabrication and characterization of double-perovskite oxide nanostructures. Mr. K. Leng is a current M. Sci. candidate at the School of Physics, Nanjing University, under the supervision of Prof. X. Zhu. His research interests include the fabrication and characterization of double-perovskite oxide nanocrystals. Mr. W. Xia, a current Ph.D. candidate at the School of Physics, Nanjing University, under the supervision of Prof. X. Zhu. He received his B.S. and M.S. degrees in condensed matter physics from Nanjing University. His research interests include the fabrication and characterization of low-dimensional perovskite manganite nanostructures. Prof. X. Zhu received his B.S., M.S., and Ph. D degrees in Materials Science from Xi'an Jiaotong University (Xi'an, China) in 1989, 1992, and 1995, respectively. He has been a full professor in condensed matter physics at the School of Physics, Nanjing University since 2006. He has published > 135 papers in prestigious international refereed journals with the SCI cited times of > 2000.

Graphical abstract

Optical absorption spectra of the Ba₂FeNbO₆ samples synthesized at different temperatures and their plots of $(\alpha hv)^2$ vs $h\nu$ curves. (a) 800°C, (b) 900°C, (c) 1000°C, and (d) 1100°C. Inset is the local optical absorption spectra, indicating the red shift of the wavelength corresponding to the optical absorption peak. The optical direct band gap energy (E_g) values (linear extrapolation of the Tauc method), are determined to be in the range of 2.12 eV - 2.25 eV.

